ISSN (O): 2393-8609
International Journal of Aerospace and Mechanical Engineering
Volume 8 – No.2, September 2021

Experimentation of a TEC-Module Cooling System using Regenerative Braking with Model Based Approach

Debarupam Gogoi
Jorhat Engineering College
Mechanical Engineering Department
debarupam@gmail.com

Akshay Kalul Saikia
Jorhat Engineering College
Mechanical Engineering Department
aksaikia12@gmail.com

Anupjyoti Burhagohain
Jorhat Engineering College
Mechanical Engineering Department
agohain00@gmail.com

Manisha Kardong
Jorhat Engineering College
Mechanical Engineering Department
kardongmanisha82@gmail.com

Subhajit Sen
Jorhat Engineering College
Mechanical Engineering Department
subhajitsen3214@yahoo.com

ABSTRACT
Conventional air conditioning system in four-wheeler vehicle consumes significant amount of fuel to run its motor. Keeping this in view, we designed an analogue working model for converting the energy otherwise lost due to friction in conventional braking into an electrical energy that can be stored in an ESD (Energy Storing Device) for running a thermoelectric cooling system. The model is mainly designed keeping in aim for four-wheeler vehicle to use the regenerative braking to run an air-cooling system inside of that without consuming extra fuel. Main work is divided into two stages, in first stage two roller brakes of diameter 3.2 cm and mass 0.075 kg each work against the rotating brake-drum of mass 1.3 kg and 14.6 cm diameter connected to a 1500 rpm and 0.75 H. P motor to convert the rotational kinetic energy into electrical energy by a dynamo of 6v. The variation of voltage due to application of brake at different rpm is validated by an oscilloscope. 0.18-amp current can be achieved around 23 v at 900 rpm of brake drum. In second stage of work, the energy is used from the ESD by the thermoelectric cooling device consisting of two sandwiched thermoelectric modules of 12v and is applied in a 1.2 cubic meter closed chamber. Result shows, temperature inside the chamber drops markedly from 40.8 degree Celsius to 28.4 degree Celsius within 3.6 minutes. COP of the system was found to be 12.02.

.

NOMENCLATURE

I_1	Moment of Inertia of Brake Drum [kg-m^2]
I_2	Moment of Inertia of Roller Brake [kg-m^2]
C_p	Specific heat of air [kJ/kg. K]
d	diameter of the shaft [mm]
m	Mass flow rate of air [kg]
N	R.P.M of shaft
R	Resistance of Heat Sink [^{o}C/W or K/W]
$SMPS$	Switch Mode Power Supply
TEC	Thermoelectric Cooling
COP	Coefficient of Performance
V_{max}	Maximum Voltage
V_{min}	Minimum Voltage
$\dot{M}$	Mass of Brake Drum [kg]
$\dot{m}$	Mass of Roller Brake [kg]
$\bar{R}$	Mean radius of Brake Drum [m]
$\bar{r}$	Mean radius of Roller Brake [m]
τ	Torque Transmitted [N-mm]
λ	Shear strength of shaft material [N/mm^2]
Ω	Power transmitted to shaft
$\dot{\omega}$	Angular velocity of Brake Drum [rad/sec]
$\hat{\omega}$	Angular velocity of Roller Brake [rad/sec]
$\Pi_{k,1}$	Kinetic Energy of Brake Drum [Joule]
$\Pi_{k,2}$	Kinetic Energy of Roller Brake [Joule]

Keywords
Regenerative braking, thermoelectric cooling, roller brake, rotational K.E., oscilloscope.

INTRODUCTION
Regenerative braking and thermoelectric cooling are two methods of conversion of energy into some useful effect from economic point of view. Regenerative braking system may be used to convert rotational kinetic energy into electrical energy and on the application of electrical energy, thermoelectric module can give cooling effect. Till now, regenerative vehicle has found its major application in electric vehicle and some hybrid vehicle. The consideration of regenerative braking in improvement of energy efficiency for electric vehicle has been discussed with two different evaluation parameters by Chen Lv et al. [1]. For improving regeneration efficiency, a modified control strategy has been carried out on design and control of a regenerative braking system for a rear driven electrified minivan and compared the outcomes with a baseline control strategy [2]. Another modified control strategy of regenerative braking on a method of braking intensity was developed and found to be effective on consideration of various slope road condition [3]. A dual control strategy [4], with bi-directional cascaded converter can increase the power stored during braking by 2.5 times and vehicle comes to a faster halt in comparison to existing control strategy. Regeneration Factor = Energy recovered to

ISSN (O): 2393-8609
International Journal of Aerospace and Mechanical Engineering
Volume 8 – No.2, September 2021

the battery during braking/Total braking energy, can be measured by reinforcement learning method on fuzzy logic model for regenerative braking [5]. It is necessary to analyse the potential for energy regeneration in cars and therefore similar study shows detailed data set representing individual car movements including elevation of a normalized vehicle model [6]. Considering energy transfer and hybrid energy distribution strategy with battery and ultra-capacitor, an optimal power allocation strategy may be developed to improve recovery and utilization efficiency of regenerative braking [7]. Here, ultra-capacitor is a rechargeable energy storing device utilized to transmit high current on acceleration and capturing regenerative braking on deceleration and during braking [8]. The regenerative energy may also be maximised by transmission downshifting. Results shows that 10.5 to 32.4% more energy conversion of regenerative braking can be obtained with downshifting [9]. Moreover, both up and down power shifting together may improve the efficiency and recovery capability during regenerative braking [10].

Now, on the other hand; if voltage is applied at the junction of the TEC module, current will flow around the circuit causing one junction to heated up and the other cooled down. This principle on which thermoelectric cooling works is known as Peltier effect [11]. While designing a Peltier cooler by experimental analysis [12] of effect of air and water parameters on exergy distribution and thermodynamic second law performance, it was found that thermoelectric cooler is suitable for warmer weather regions than moderate climate. The basic concept of thermoelectric and its recent material are coming to focus under research area such as application of thermoelectric module and generator with structure optimization for low temperature recovery, heat resource and application of thermoelectric cooler including thermoelectric model [13]. Again, for building space cooling operation, a numerical model for the thermoelectric cooling system has been developed [14] where normal current pulse operation of the thermoelectric cooler is modified by adding pulsation of heat transfer coefficient of hot side to it. Moreover, improving performance of TEC module has been a continuous effort of the researchers in this field. The Performance enhancement is also dependent on thermoelectric geometry and parametric optimization of the module [15]. In a study, the maximum cooling capacity, temperature difference, and co-efficient of performance can be markedly improved in two segmented thermoelectric coolers [16]. Also, tubular shaped thermoelectric module shows better performance than flat shaped one. Similarly, cooling capacity and coefficient of performance may increase up to 35.73% and 21.59% in a non-constant cross section thermoelectric cooler [17, 18]. Again, in some special cases, cooling performance may be enhanced by using radiative sky cooler [19] on both heating and cooling sides of the thermoelectric module to increase additional cooling power and heat dissipation respectively. Like Peltier effect, Thomson effect has also considerable effect on cooling performance of micro thermoelectric cooler [20] while considering interfacial and size factor. The positive Thomson coefficient may slightly increase the cooling performance of a thermoelectric device [21]. On the other hand, position of the thermoelectric module inside the cooler and number of modules has vital role in cooling performance. It was found that wall position is most effective as compared to the other positions like, top, bottom or middle inside the cooler [22]. Similarly, a two-jointed thermoelectric module has better cooling performance than a single one. It has been shown in the study that six-jointed modules have 100% higher coefficient of performance than two-jointed modules [23] for the same input electrical power. In this project, two-jointed thermoelectric module has been considered enough for two or four seated vehicles.

1. METHODOLOGY

A thermoelectric cooling model is developed for a four-wheeler vehicle which will be run by regenerative braking power from the vehicle without consuming any extra fuel. The performance of the model is investigated at two stages: regenerative braking unit and thermoelectric cooling unit. In first stage, the energy lost due to application of brake is converted into current and the e.m.f generated is validated by an oscilloscope. In second stage of work, the stored electrical energy is being utilized for cooling effect by two TEC plates inside a chamber and temperature dropped is recorded. The procedures adopted for the work from beginning to end is reflected in the Flow-chart shown by Fig. 1.

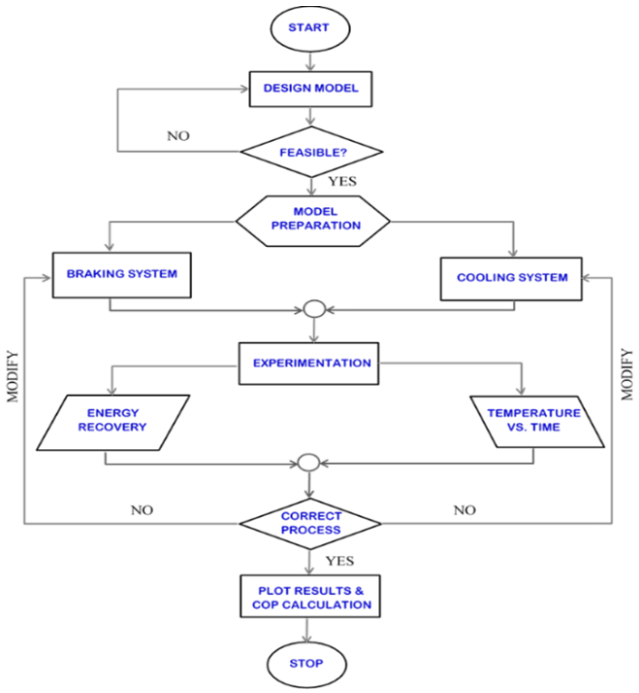

Figure 1: Flow Chart showing the methodology of work

2. EXPERIMENTAL SET-UP

To conduct the experiment, a test model was set up as: A frame (80×29.5cm) is made through welding process and it includes two stands of height 43cm to carry the two bearings. A shaft passes through the bearings and is fitted to the brake drum of 14.6 cm diameter and mass 1.3 kg. The shaft is coupled to the shaft of a motor (1500 rpm, 0.75 HP) through clutch coupling. Roller brakes made of P.V.C are used of diameter 3.2 cm and mass 0.075 kg each. Dynamos of 6v are fitted to the roller brake shafts to produce the current during brake application. Two 12 V TEC plates are sandwiched between two heat sinks with the help of thermal grease. A suction pipe with fan fitted at one of its ends is fixed in such a way that the air sucked in from the atmosphere strikes the cold side heat sink. Fans are also used to discharge the cold air from the chamber. The cooler is insulated with the help of Styrofoam. A chamber of 1 cubic meter is used as cooling space to analyse the working of the cooler. Fig. 2 shows the first angle projection view of wire-frame model and isometric view of solid model of the prototype.

ISSN (O): 2393-8609
International Journal of Aerospace and Mechanical Engineering
Volume 8 – No.2, September 2021

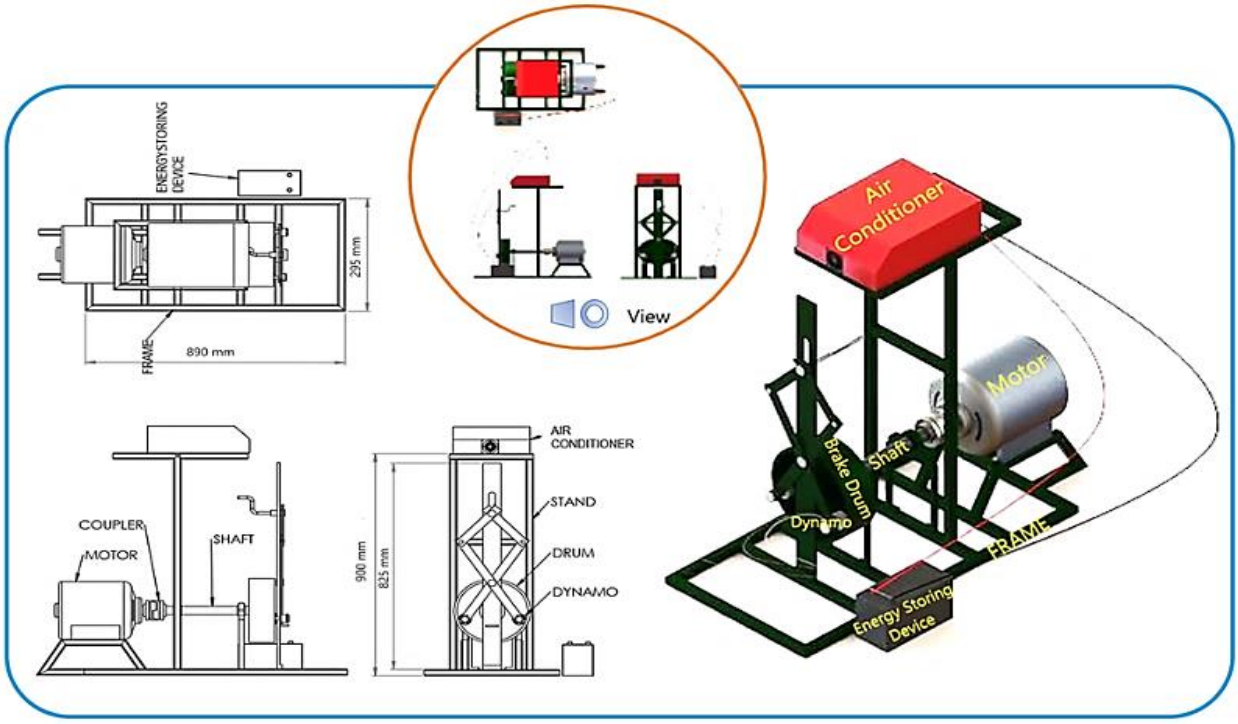

Figure 2: Schematic of the Test-Model

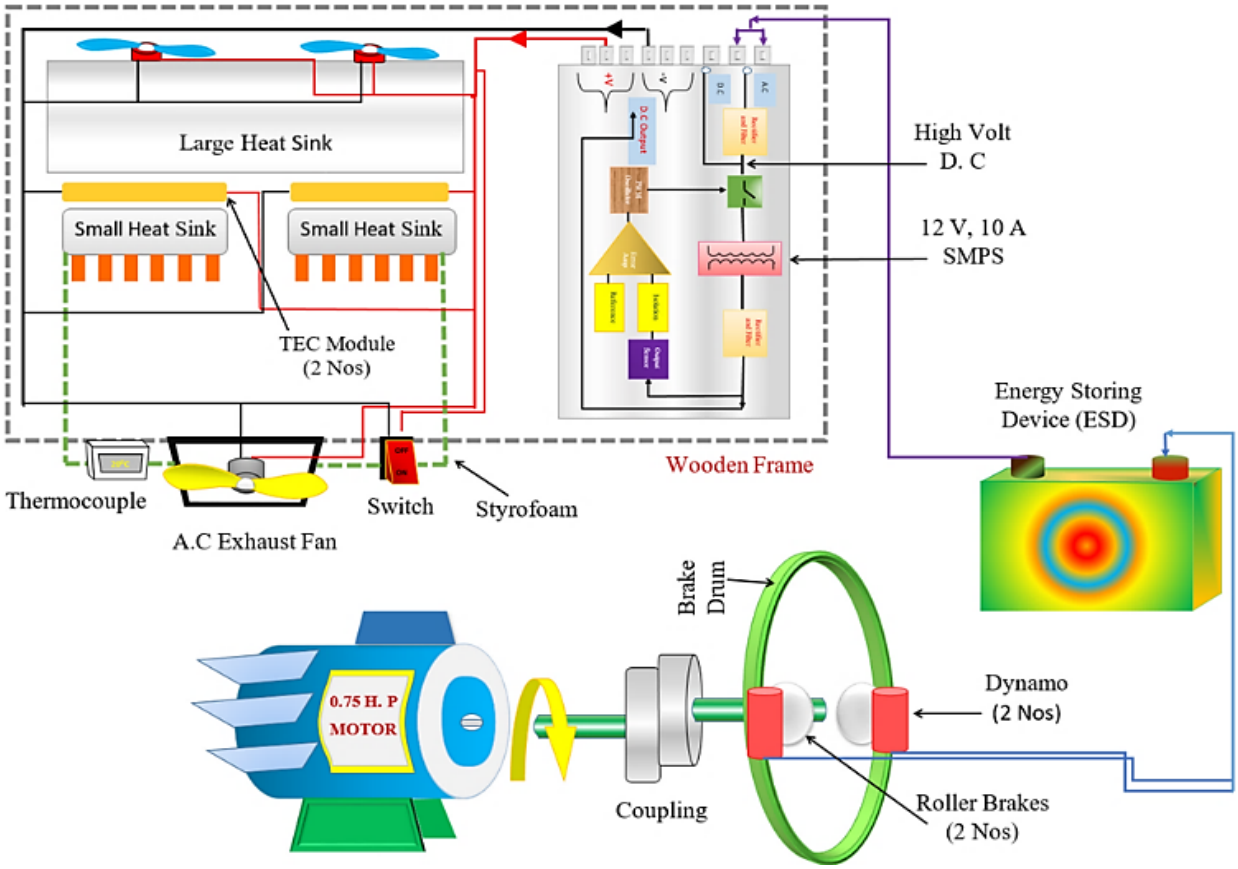

Figure 3: Experimental set up of regenerative and thermoelectric unit

The model mainly consists of two units: 1) Regenerative or braking unit and 2) Thermoelectric or cooling unit. The regenerative unit consist of motor, shaft, coupling, Brake drum, Roller brake, Dynamo and ESD. The thermoelectric

ISSN (O): 2393-8609
International Journal of Aerospace and Mechanical Engineering
Volume 8 – No.2, September 2021

unit comprises of ESD, SMPS, Heat sinks, TEC modules, cooling and exhaust fans etc. Detailed connection between the two unis is shown in Fig. 3

The materials and specification of the parts used in the actual model are listed in Table 1

Table 1: List of materials used in fabrication and assembling of the model of our project.

Sl .no	Name of items	Specification	No of parts
1	Brake drum	14.6 cm	1
2	Shaft	20 mm	1
3	Bearing	20 mm U.C bearing	2
4	Jaw coupling	-	1
5	Motor	1500rpm,0.75hp	1
6	Roller brakes of P.V.C Dynamo	3.2cm	2
7	T.E.C plate	6V	2
8	Heat sink	12V	2
9	Fans	85.4mm×85.4mm×41.5mm	3
10	P.V.C pipe	12V,13 A	4
11	Cardboard	-	1
12	Styrofoam	31mm×37mm×17mm	1
13	ESD	-	1
14	Transformer	12V	1
15		0-12 Ma	1

2.1 Regenerative Unit

After fabricating the models, we carried out the required experiments to find out the energy recovered by the use of regenerative braking and the cooling capacity of the thermo-electric cooler. For determining the energy recovered, the mass and diameter of brake drum and roller brakes were measured in order to find out the moment of inertia of each.

The brake drum and the roller brake can be considered as a general rigid body constituted with 'N' numbers of particles and rotating about an axis. Let r_i be the radius of i[th] particle from point 'O' as shown below:

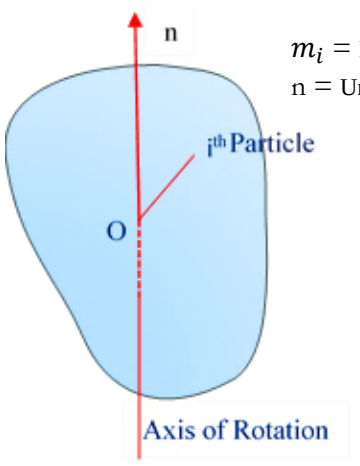

The moment of inertia for the rigid body about its axis of rotation can be expressed a

$$\sum_i m_i |r_i \times n|^2 = I \quad (1)$$

Here, $(r_i \times n)$ is the perpendicular distance of the i[th] particle from the axis of rotation. Now, moment of inertia for the brake drum and roller brake can be written in the form:

For Brake Drum,

$$I_1 = 0.5 M R^2 \quad (2)$$

For Roller Brake,

$$I_2 = 0.5 m r^2 \quad (3)$$

The motor runs the driving shaft and thereby the brakes drum which varies in between 100 - 900 rpm. The speed of roller brake and voltage as well as current generated by the dynamos were noted down with multi-meter (VOM) and digital tachometer. The kinetic energy of the brake drum and the roller brakes can be found out as follows: Referring to the rigid body above, the kinetic energy of motion of a system of particles is defined by,

$$\Pi_K = 0.5 \sum_i m_i v_i^2 \quad (4)$$

Here, v_i is the linear velocity of the i[th] particle relative to point 'O'. From vector geometry,

$$v_i = \vec{\omega} \times r_i \quad (5)$$

So, Eq. (4) can be re-written as:

$$\Pi_K = 0.5 \sum_i m_i \, v_i . (\vec{\omega} \times r_i)$$
$$= 0.5 \sum_i m_i \, \vec{\omega} . (r_i \times v_i) \quad (6)$$

Little rearranging Eq. (6), we find that;

$$\Pi_K = 0.5 \, \vec{\omega} . [\sum_i m_i \, (r_i \times v_i)]$$
$$= 0.5 \, \vec{\omega} . \mathrm{L} \quad (7)$$

Where, L is the linear momentum vector about point 'O' and it is written in terms of moment of inertia tensor I and $\vec{\omega}$ as,

$$L = \sum_i m_i (r_i \times v_i) \quad (8)$$
$$= \sum_i m_i [r_i \times (\vec{\omega} \times r_i)]$$
$$= \sum_i m_i \left[\vec{\omega} r_i^2 - (r_i . \vec{\omega}) r_i\right] \quad (9)$$
$$= \{\sum_i m_i \left[r_i^2 - r_i (r_i .)\right]\} \vec{\omega} \quad (10)$$

In terms of components of vectors,

$$L = i L_x + j L_y + k L_z \quad (11)$$

From Eq. (9),

$$L = \sum m_i \left[(i\omega_x + j\omega_y + k\omega_z) r_i^2 - (r_i . \vec{\omega})(i x_i + j y_i + k z_i)\right] \quad (12)$$

Emphasizing the linearity by introducing I_{xx} , I_{xy} , I_{xz} , I_{yx} , I_{yy} , I_{yz} , and I_{zx} , I_{zy} , I_{zz} ; from equations (11) and (12) we can write:

$$L_x = I_{xx}\omega_x + I_{xy}\omega_y + I_{xz}\omega_z$$
$$L_y = I_{yx}\omega_x + I_{yy}\omega_y + I_{yz}\omega_z \quad (13)$$
$$L_z = I_{zx}\omega_x + I_{zy}\omega_y + I_{zz}\omega_z$$

In matrix form,

$$\begin{pmatrix} L_x \\ L_y \\ L_z \end{pmatrix} = \begin{pmatrix} I_{xx} & I_{xy} & I_{xz} \\ I_{yx} & I_{yy} & I_{yz} \\ I_{zx} & I_{zy} & I_{zz} \end{pmatrix} \begin{pmatrix} \omega_x \\ \omega_y \\ \omega_z \end{pmatrix} \quad (14)$$

$$\text{Or,} \quad L = I\vec{\omega} \quad (15)$$

So, angular momentum of brake drum and brake can be written as:

$$I_1 \dot{\omega} \quad \text{(for brake drum)} \quad (16)$$
$$\text{And} \quad I_2 \dot{\omega} \quad \text{(for brake)} \quad (17)$$

ISSN (O): 2393-8609
International Journal of Aerospace and Mechanical Engineering
Volume 8 – No.2, September 2021

From Eq. (7), kinetic energy of the rigid body is

$$\Pi_K = 0.5\,\vec{\omega}.I.\vec{\omega} = 0.5\,I\,\vec{\omega}^2 \quad (18)$$

Now, the expression for kinetic energy of brake drum and roller brake may be written as,

For Brake Drum,

$$\Pi_{K,1} = 0.5\,I_1\dot{\omega}^2 \quad (19)$$

For Roller Brake,

$$\Pi_{K,2} = 0.5I_2\dot{\omega}^2 \quad (20)$$

Figure. 4 shows the regenerative unit in which, how the essential parts were assembled and connected with each other is shown.

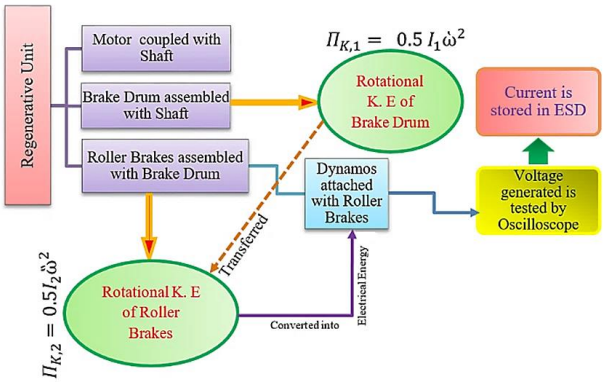

Figure 4: Regenerative unit showing the assembled parts connected with each other.

Total kinetic energy of the two roller brakes:

$$\Sigma_{n=1}^{2}\ 0.5I_2\dot{\omega}^2 \quad (21)$$

Since the roller brakes were initially at rest, the kinetic energy of the brakes must have been derived from the drum after the application of the brakes. Fractions of energy recovered were calculated thereafter.

Highest speed to be analysed = 1000 rpm.

$$\text{Torque generated, } \tau = \frac{\Omega\times 60}{2\pi N} \quad (22)$$

i.e. $\tau = (60\times 559.275) / (2\pi\times 1000)$

$\Rightarrow \tau = 5.340$ Nm $= 5340$ N-mm

Now,

Shear strength of mild steel, λ = 240 MPa = 240 N/mm^2, assuming factor of safety to be 4,

Permissible shear strength of mild steel, λ= 240/4 = 60 N/mm^2

So, shear strength of mild steel,

$$\lambda = \frac{16\,\tau}{\pi d^3} \quad (23)$$

$\Rightarrow$d = 7.68 mm

So, standard shaft diameter = 10 mm as per Design Data Handbook [24].

Mass of the drum = 1.3 kg, Diameter of drum = 0.146 m, Radius = 0.073 m

M.I. of drum, from Eq. (2)

$$I_1 = 0.5\dot{M}\dot{R}^2 = 0.00346 \text{ kg-m}^2$$

Mass of brakes = 0.075 kg each, Diameter = 0.032 m

M.I. of brakes, from Eq. (3),

$$I_2 = 0.5\dot{m}\bar{\dot{r}}^2 = 3.84 \times 10^{-5} \text{ kg-m}^2.$$

At 100 rpm of Brake Drum, RPM of brake,

$$\dot{\omega} = \frac{\dot{\omega}\times\bar{\dot{R}}}{\bar{\dot{r}}} \quad (24)$$

2.2 Results, Discussion and Verification (Regenerative Unit)

Rotational K.E. of the Drum, from Eq. (19)

$$\Pi_{K,1} = 0.5\,I_1\dot{\omega}^2$$

$$= 0.189 \text{ J}$$

Rotational K.E. of Brake, from Eq. (20)

$$\Pi_{K,2} = 0.5I_2\dot{\omega}^2$$

$$= 0.0437 \text{ J}$$

The following Table 2 is prepared throughout the process at nine different rpm of brake drum ranging from 100 to 900 at an interval of 100 rpm.

Table 2: Rotational K.E. of Brake Drum and brake at different RPM of Brake Drum

RPM (Brake Drum)	Rotational K.E. (Drum)	Rotational K.E. (One Brake)	Percentage Energy Recovered
100	0.189	0.0437	23.12
200	0.757	0.175	23.11
300	1.705	0.394	23.1
400	3.03	0.70	23.10
500	4.74	1.094	23.08
600	6.822	1.58	23.16
700	9.284	2.15	23.15
800	12.12	2.8	23.1
900	15.35	3.55	23.13

Again, nine samples of angular momentum of brake and brake drum against their r.p.m, using Eq. (15) and Eq. (24) have been shown in Fig. 5 in time and frequency domain analysis. The normalized frequency is in log scale and magnitude is in decibel.

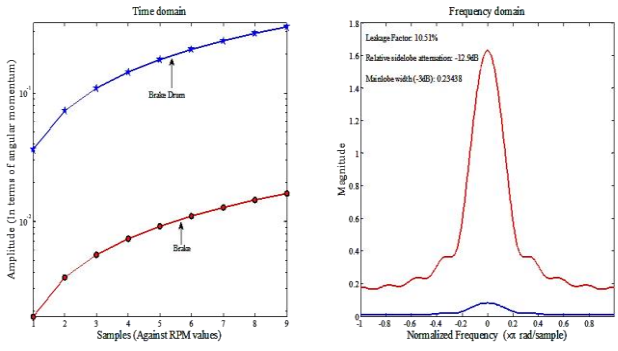

Figure 5: Angular momentum of brake and brake drum in time and frequency domain analysis

The distribution of angular momentum of the roller brake which have significant contribution in braking has been shown in contour plot with corresponding best surface fit model (poly13) in Fig. 6.

ISSN (O): 2393-8609
International Journal of Aerospace and Mechanical Engineering
Volume 8 – No.2, September 2021

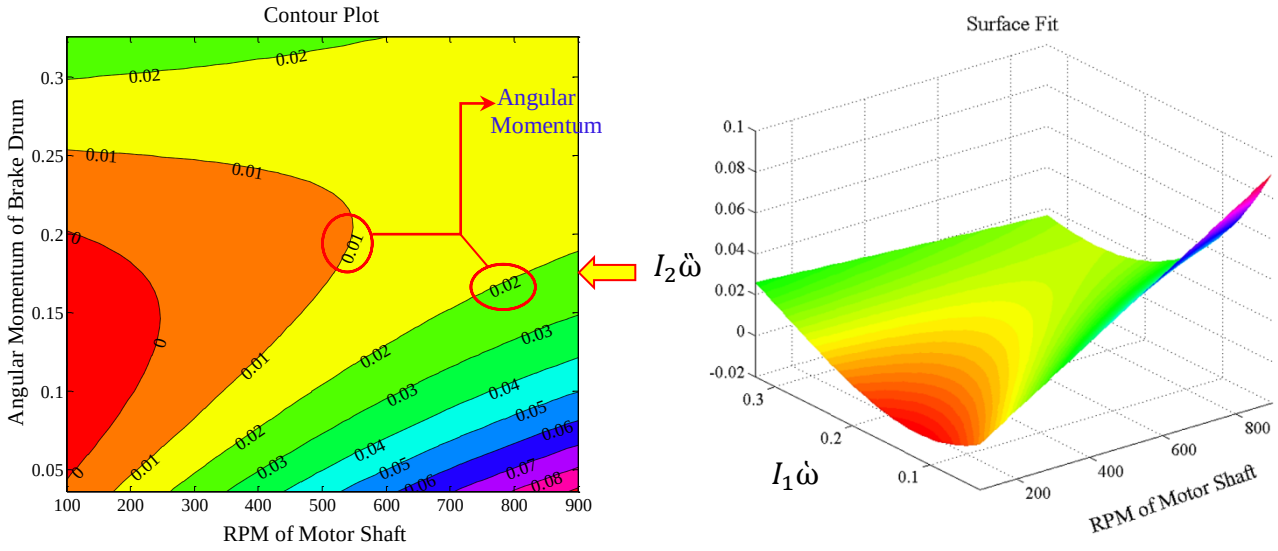

Figure 6: Distribution of angular momentum of brake against different rpm of motor shaft and corresponding surface model.

The energy stored in the battery is proportional to the energy recovered during regenerative braking. The regeneration factor may be defined as the ratio between the energy recovered to the battery and the total braking energy. The graphical representation of results listed in table 2 to show percentage of energy recovered when rotational kinetic energy is transferred from brake drum to roller brake is shown in Fig. 7 below.

The distribution of energy recovered as a function of kinetic energy of brake drum and brake has been shown in contour plot and its corresponding surface fit model with bi-harmonic Interpol function (no residual). Plot is shown in Fig. 8.

This recovered energy is converted into current by the dynamo with induced e.m.f. Before carrying further investigation, the voltage generated was checked by multi-

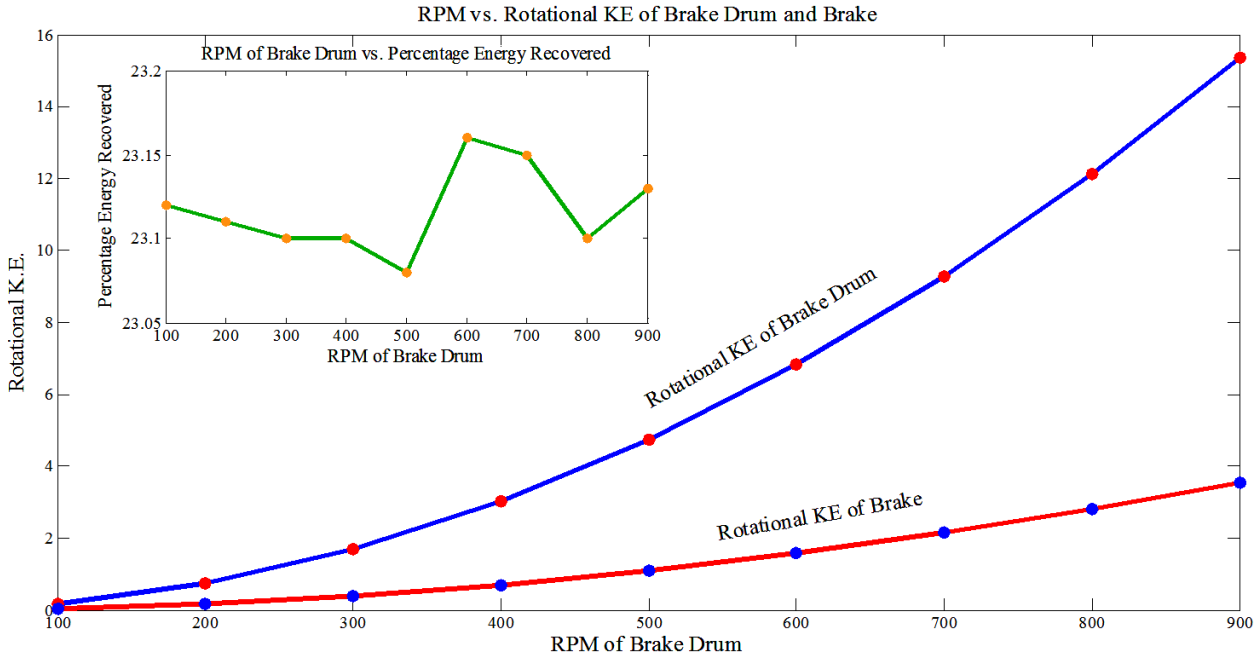

Figure 7: Rotational K.E. of brake Drum & Brake vs. RPM of Brake Drum and Percentage of Energy Recovered

The diverging gap between the rotational kinetic energies of brake drum and brake shows how much useful energy has been wasted as frictional or heat energy and other ways. On the other hand, plot (inside window) shows optimal energy recovered by one brake unit is around 600 rpm of motor shaft, assuming no torque lost during transmission to brake drum.

meter and further validation were done with an oscilloscope.

During the test in oscilloscope, it has been found that a varying current is existing in the oscilloscopic graphs. This is because as we apply the brakes, the speed of the brake drum goes on changing and hence the speed of the dynamo shaft rotation also changes. At higher speed higher voltages are

ISSN (O): 2393-8609
International Journal of Aerospace and Mechanical Engineering
Volume 8 – No.2, September 2021

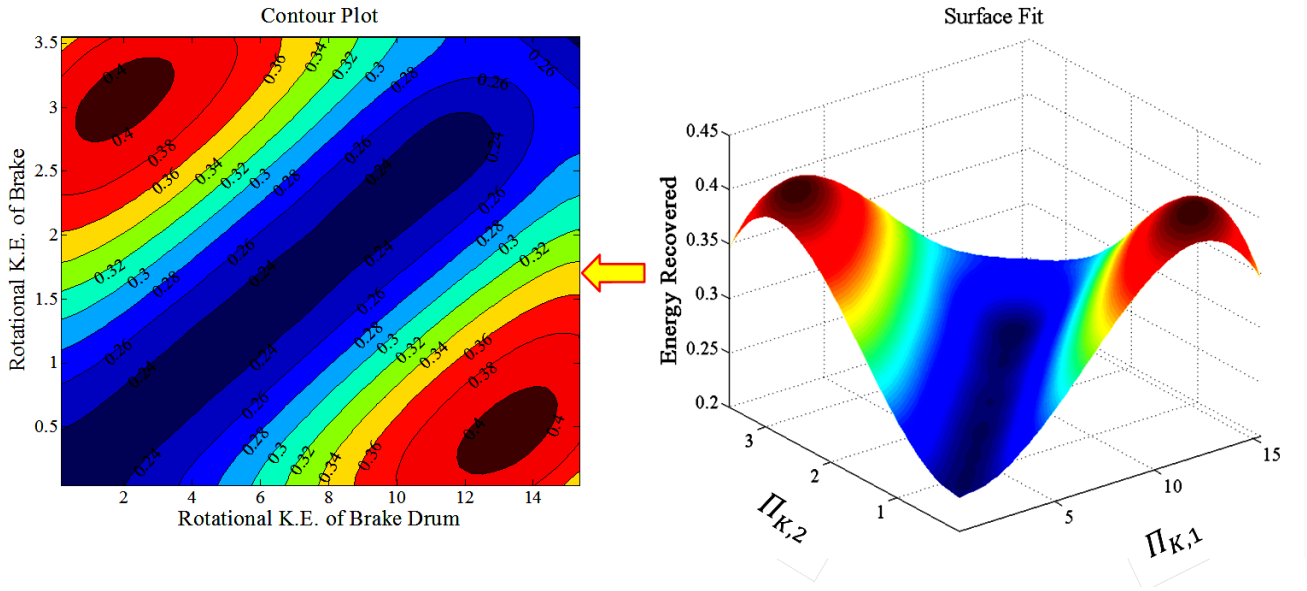

Figure 8: Plot showing energy recovered during regenerative braking as a function of K.E. of brake drum and brake.

found to develop due to the very same reason. The *Vmax*, *Vmin* for different RPM are shown in the graphs itself in Fig. 9.

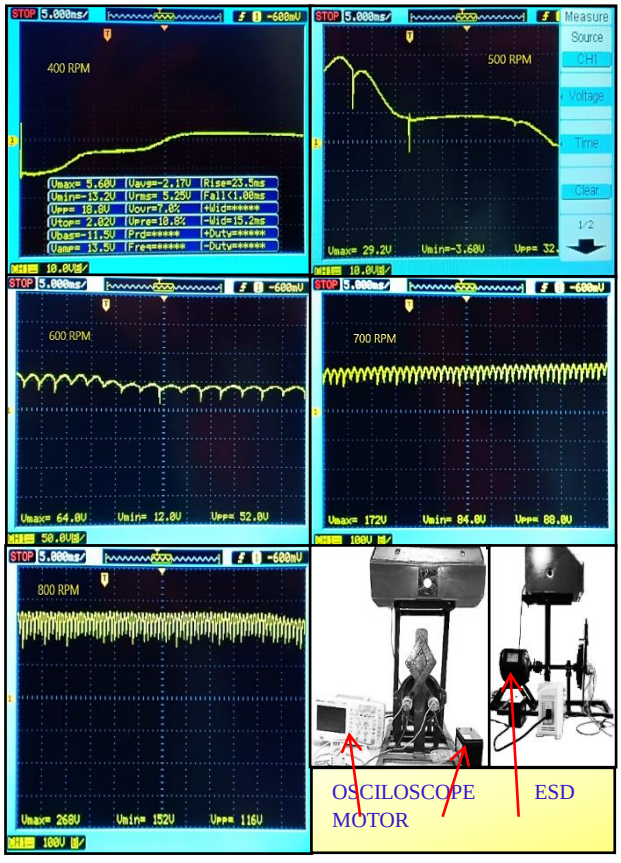

Figure 9: Oscilloscopic Graphs of Voltage at Different RPM of Motor Shaft

The measured value of voltage in volt and current produced (Amp) by dynamo at different RPM of Brake Drum and Brake are listed in Table 3.

Table 3: Rpm of Brake Drum and Brake vs. Current and Voltage

Rpm (Brake Drum)	Rpm (Brake)	Voltage	Current
100	456.25	4.7	0.1
200	912.5	6.1	0.11
300	1368.75	10.3	0.11
400	1825	11.7	0.13
500	2281.25	16.4	0.14
600	2737.5	17.4	0.14
700	3193.75	18.5	0.14
800	3650	19.4	0.16
900	4106.25	23.6	0.18

The graphical representation of voltage generated at different RPM of brake drum and brake can be compared in Fig. 10 shown below.

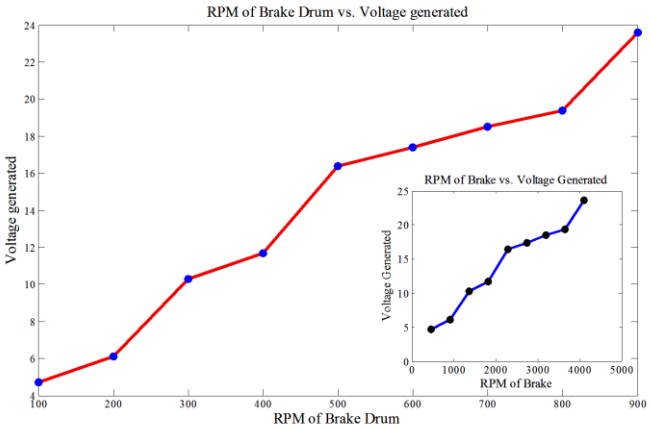

Figure 10: Voltage generated by terminals at different RPM of Brake drum and Brake.

ISSN (O): 2393-8609
International Journal of Aerospace and Mechanical Engineering
Volume 8 – No.2, September 2021

Similarly, current produced by the dynamo at different RPMs of Brake and Brake drum can be compared in Fig. 11.

Also, contrary to energy recovered; current production is showing constancy from 500 rpm to 700 rpm although voltage

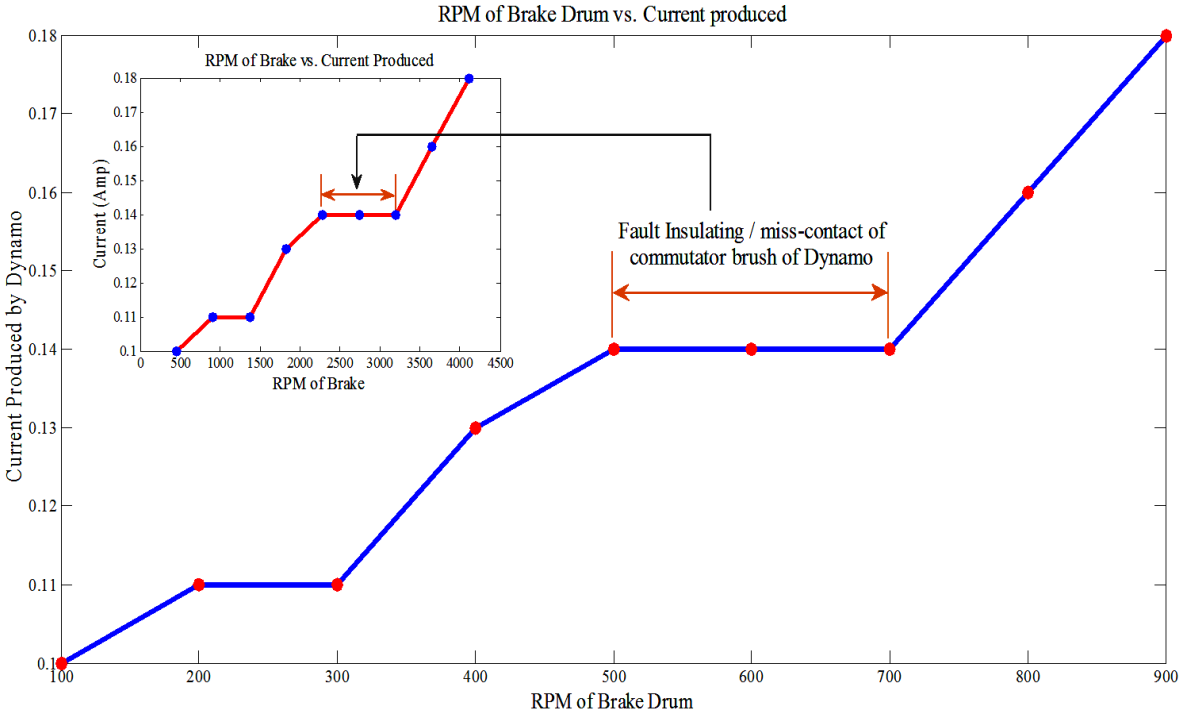

Figure 11: Current produced at different RPMs of Brake drum & Brake

The total energy recovered by the two brake units can be determined using Eq. (21); but instead, current converted by

generation is regular. This may happen on account of fault insulating or miss-contact of commutator brush of the dynamo. Distribution of current as a function of rpm of motor

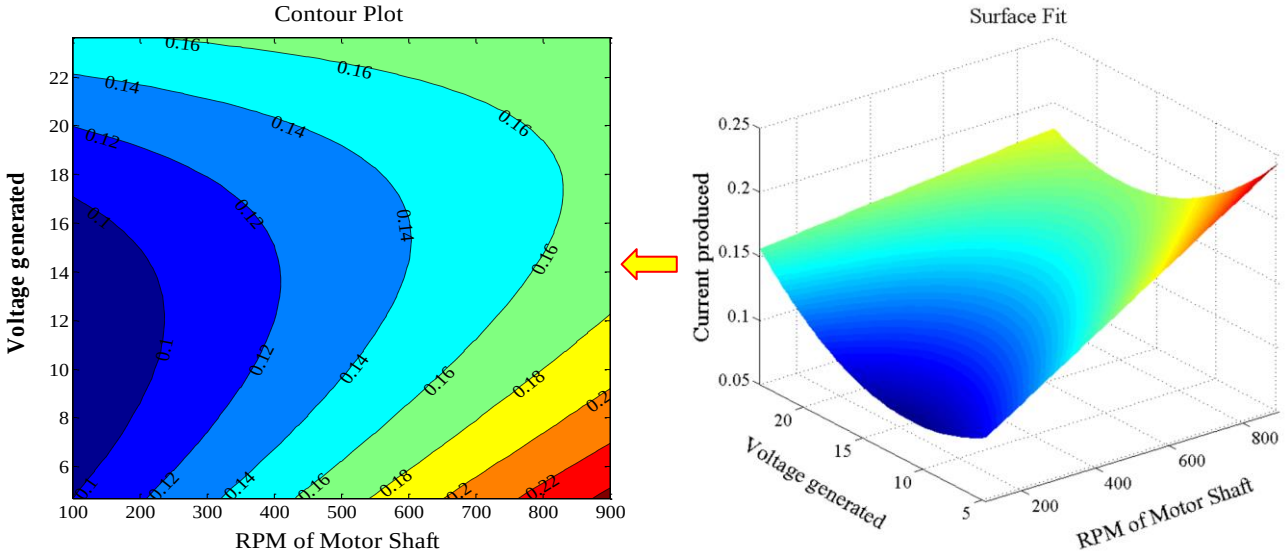

Figure 12: Plot showing current distribution against RPM of motor shaft and voltage generated by dynamo

dynamos are showing highest at 900 rpm as seen from Fig. 12.

shaft and voltage generated by dynamo has been shown in contour plot with corresponding surface fit model in Fig. 12.

ISSN (O): 2393-8609
International Journal of Aerospace and Mechanical Engineering
Volume 8 – No.2, September 2021

From Table 2 and Table 3, a comparative study between rotational kinetic energies of brake drum and brake with voltage generated at different RPM of brake drum can be done. Similarly, rotational kinetic energies of brake and brake drum for current produced by the dynamometer at different RPMs of brake drum can be shown in Fig. 13

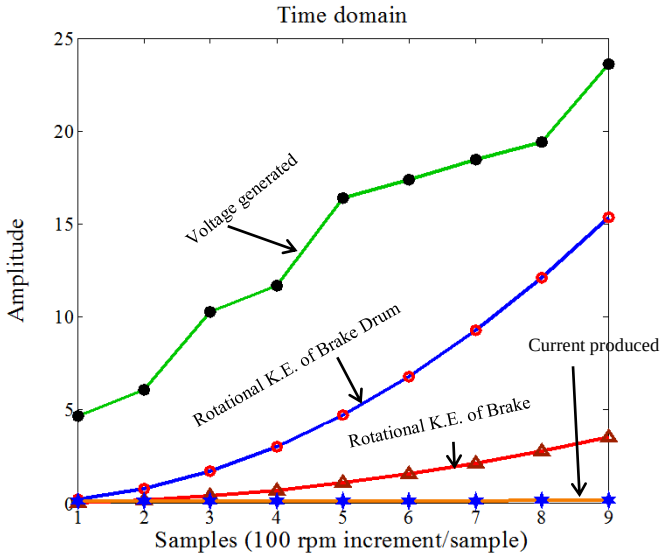

Figure 13: Comparisons of Rotational KE of Brake & Drum with Voltage & Current at different RPMs

Again, Distribution of current as a function of kinetic energy of brake and voltage generated by dynamo has been shown in contour plot with corresponding surface fit model (poly22) in Fig. 14.

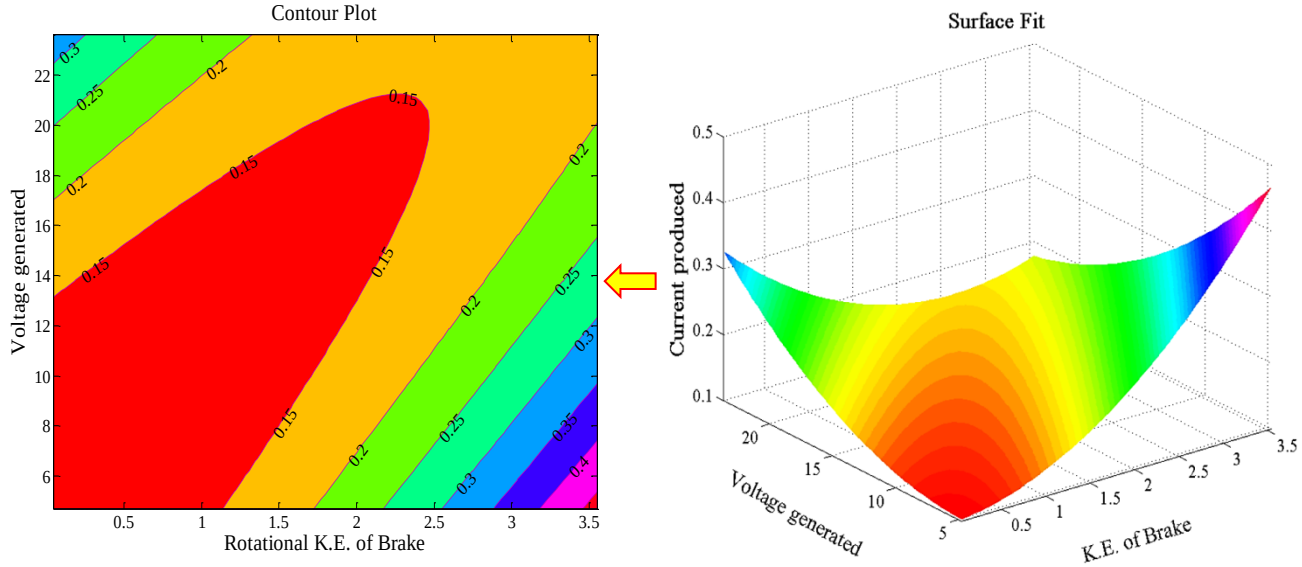

Figure 14: Distribution of current against rotational kinetic energy of brake and voltage generated by dynamo.

The voltage generated and current produced may also be validated by using 'Karl Pearson' model. Here, the coefficient of correlation is determined by:

$$r = \frac{\sum \tilde{V}\tilde{I}}{\sqrt{(\sum \tilde{V}^2)(\sum \tilde{I}^2)}} \quad (25)$$

Here, $\tilde{V} = V$ - mean and $\tilde{I} = I$ – mean, and value of correlation coefficient is found to be 0.96.

2.3 Cooling Unit

The 12 V, 10 A SMPS gets D. C voltage from the ESD. The connection is shown in Fig. 3.

The output of the SMPS is connected with cooling fans, TEC modules, exhaust fans, thermocouple, switch etc. All positive connections are assembled together (red wires) and connected

ISSN (O): 2393-8609
International Journal of Aerospace and Mechanical Engineering
Volume 8 – No.2, September 2021

to positive terminal. Similarly, all negative connections (black wires) are collectively attached with the negative output terminal of the SMPS as shown in Fig. 3. Relationship among different parts of cooling unit is shown in Fig. 15. For finding appropriate TEC module in thermoelectric cooling, factors to be given importance are:

The temperature of the cold side of the TEC is T_c, to which the object to be cooled comes in contact with. Here the object is air inside the car and has to be cooled when passed through aluminium heat sinks.

The hot side temperature (T_h) is mainly the temperature of the ambient air in surroundings to which heat is being rejected.

The difference between the two temperatures T_c and T_h is noted as ΔT which should pose much accuracy for operating the cooling system in desirable range. The equation of ΔT is written as:

$$\Delta T = T_h - T_c \quad (26)$$

Similarly, system ΔT may also be expressed in terms of temperature difference between ambient and load to be cooled.

The amount of heat to be removed or absorbed (Q_c) by the cold side of the TEC is expressed in terms of mass flow rate of air, specific heat of air and temperature difference. Here the temperature difference is system ΔT

$$Q_c = mC_p\Delta T \quad (27)$$

The hot side of TEC plate require heat sink to dissipate the heat. For a set of ambient temperature and cooling load temperature, thermal resistance of heat sink could vary the ΔT and thereby could increase the current flow across the TEC. Thermal resistance is a measure of the capability of heat sink to dissipate heat. Thermal resistance may be expressed as:

$$R = \frac{(T_h - \Delta T)}{Q_h} \quad (28)$$

R is the thermal resistance (in $^oC/W$ or K/W) Expression for heat load into heat sink is given as:

$$Q_h = Q_c + P_e \quad (29)$$

$$P_w = IV \quad (30)$$

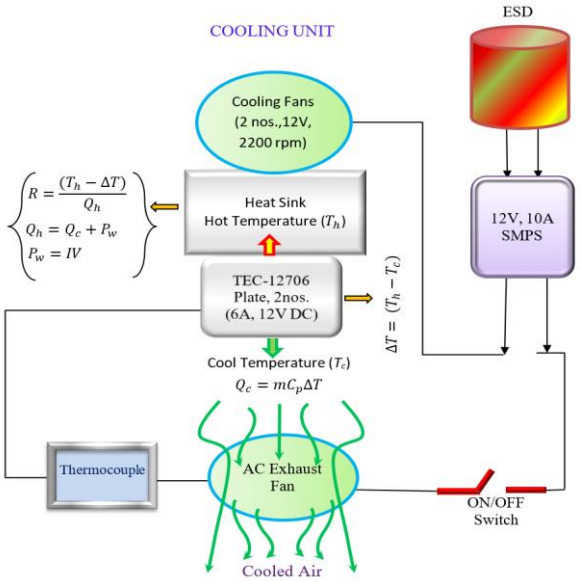

Figure 15: Relationship among different parts of cooling unit.

The product of required voltage and current may determine the power of TEC. Temperature control which is generally based on cold side for a cooling system, can be maintained by incorporating a thermostat included on-off or control technique.

For determining the cooling capacity of the thermo-electric cooler, we take a chamber of 1.2 cubic meter as the space to be cooled. We insulate the chamber using Styrofoam and attach the cooler with the chamber. In order to increase the temperature of the chamber we combust coal inside the chamber till the temperature inside reaches 40.8 degree Celsius. After the temperature has been raised to a desirable level, we take out the coal from the chamber and switch on the cooler. The corresponding drop of temperature of the chamber with respect to time and temperature drop of heat sink with respect to time is noted down. The heat transfer rate and the COP are calculated.

2.4 Results, Discussion and Verification (Cooling Unit)

Table 4 is prepared to list temperature drop against time in sec.

Table 4: Temperature drop in chamber, body and heat sink with respect to time

Samples	Time(sec)	Chamber Temp.	Body temp.	Heat sink
1	0	40.8	38	23.6
2	10	39.8	37.6	20.1
3	20	38.5	36.8	18.8
4	30	37.3	36	18
5	40	36.1	35.2	17.5
6	50	35	34.4	17.2
7	60	33.9	33.7	16.9
8	70	33.1	32.4	16.8
9	80	32.4	32	16.7
10	90	31.8	31.4	16.7
11	100	31.3	30.8	16.7
12	110	30.8	30.3	16.7
13	120	30.5	29.8	16.7
14	130	30.1	29.4	16.7
15	140	29.8	28.9	16.6
16	150	29.6	28.6	16.6
17	160	29.5	28.2	16.6
18	170	29.3	27.9	16.6
19	180	29.2	27.5	16.6
20	190	29	27.2	16.6
21	200	28.9	26.9	16.6
22	210	28.8	26.5	16.6
23	220	28.4	26.3	16.6

The chamber temperature is measured by incorporating a thermometer inside of it. The body temperature is measured with a thermocouple attached to the A.C exhaust fan as shown in Fig. 3. The noted temperature drops listed in table 4 against time, have been graphically uploaded in Fig. 16 to give a better picture for understanding.

ISSN (O): 2393-8609
International Journal of Aerospace and Mechanical Engineering
Volume 8 – No.2, September 2021

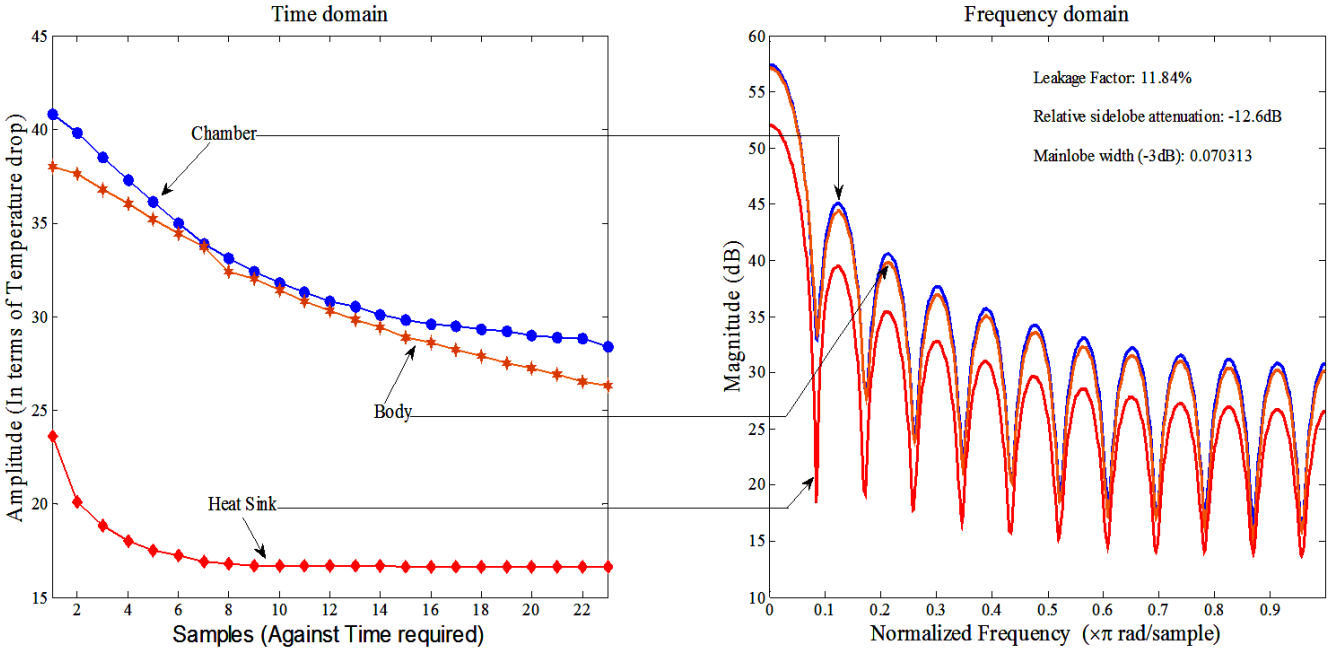

Figure 16: Plot showing temperature drop of chamber, body and heat sink against time in sec.

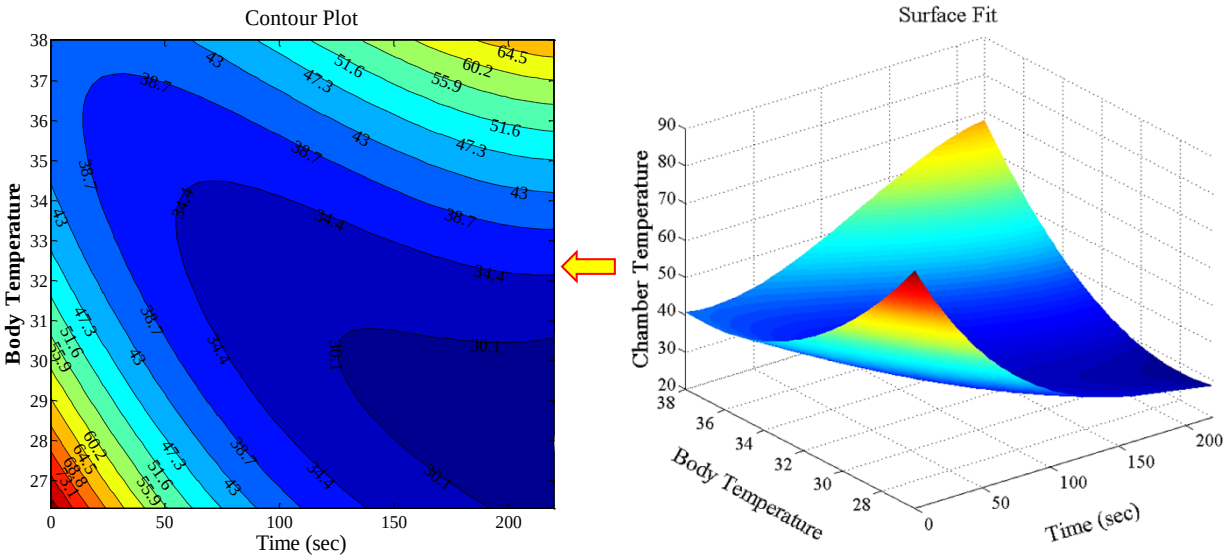

Figure 17: Surface and Contour plot for best polynomial in chamber and body temperature

From experiments of cooling unit, the chamber temperatures reading (by a thermometer) are not much differ from the recorded body temperatures (by a thermocouple connected to exhaust fan) as seen from Fig.16. The minimum heat sink temperature is limited to 16 degrees Celsius.

The chamber temperature and body temperature are compatible with best surface fit in 3rd and second order polynomial in 'x' and 'y' values. Fig.17 shows the surface fit and its corresponding contour plot.

2.4.1 Determination of COP

Temperature of the plate when cooled, T_c = 16.7°c.

Temperature of the hot chamber, T_0 = 40.8 °c.

Coefficient of heat transfer for air, h = 100 W/m² °c.

Heat transfer per unit area, $q = h(T_0 - T_c)$ (31)

= 2410 W/ m².

Coefficient of performance of the cooler,

$$\text{COP} = \frac{T_o}{(T_o - T_c)} \quad (32)$$

=12.02.

3. Conclusion:

Because of very little difference between body temperature and chamber temperature (Fig. 16) and markedly temperature drops from 40 degrees Celsius to 28 degrees Celsius within four minutes inside a 1.2 cubic meter chamber, the concept may be applied in practical situation. We have selected the 12

ISSN (O): 2393-8609
International Journal of Aerospace and Mechanical Engineering
Volume 8 – No.2, September 2021

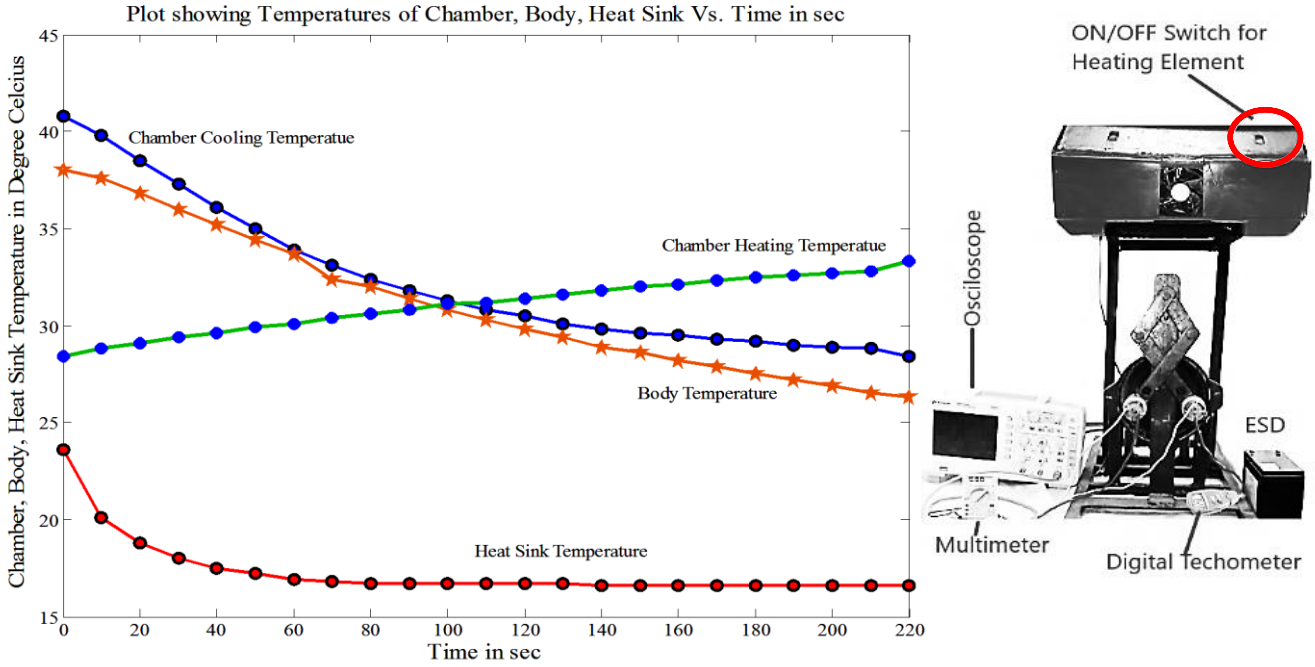

Figure 18: Plot showing cooling and heating temperature inside the chamber versus time

V, 10 A SMPS, as the input power source (D.C) from the ESD and enters the high frequency switch without passing through the rectifier in it. Similarly, the reason for using roller brake in our prototype is that, it is convenient to assemble with the dynamo. We are concentrating on combination of experiments through regenerative braking to thermoelectric cooling. In our actual model, there is also setup for heating the chamber with a heating element. Heating the chamber with filament results in raising the inside temperature from 28.4^0C to 33.3^0C in 3 minutes 40 seconds as shown in Fig. 18. The plot is modification of Fig. 16.

A maximum of four and minimum of two brake drums can be utilized in a four-wheeler vehicle for more current production as compared to a single brake drum in the prototype model.

Acknowledgement

The experiment was conducted at Jorhat Engineering College, Jorhat; 26.757874 Latitude and 94.209824 Longitude. We acknowledge to Mechanical Engineering Department and staff members of mechanical engineering laboratory of Jorhat Engineering College, who directly or indirectly help us to complete the project.

ORCID

Debarupam Gogoi https://orcid.org/0000-0002-1503-8605

References

[1] L. Chen, J. Zhang, L. Yutong, Y. Yuan, "Mechanism analysis and evaluation methodology of regenerative braking contribution to energy efficiency improvement of electrified vehicles", *Energy Conversion and Management*, vol. 92, pp. 469-482, Mar. 2015. DOI: 10.1016/j.enconman.2014.12.092.

[2] Z. Junzhi, L. Yutong, L. Chen, Y. Yuan, "New regenerative braking control strategy for rear- driven electrified minivans", *Energy Conversion and Management*, vol. 82, pp. 135-145, Jun. 2014. DOI: 10.1016/j.enconman.2014.03.015.

[3] L. Zhang, X. Cai, "Control strategy of regenerative braking system in electric vehicles", *Energy Procedia*, vol. 152, pp. 496-501, Oct. 2018. DOI: 10.1016/j.egypro.2018.09.200.

[4] S. Mehta, S. Hemamalini, "A Dual Control Regenerative Braking Strategy for Two-Wheeler Application", *Energy Procedia*, vol. 117, pp. 299-305, Jun. 2017. DOI: 10.1016/j.egypro.2017.05.135.

[5] R. Maia, J. Mendes, R. Araujo, M. Silva, U. Nunes, "Regenerative braking system modelling by fuzzy Q-Learning", *Engineering Applications of Artificial Intelligence* 93 (2020)03712, DOI:10.1016/j.engappai.2020.10372.

[6] L.-H. Bjornsson, S. Karlsson, "The potential for brake energy regeneration under Swedish conditions", *Applied Energy*, vol. 168, pp. 75-84, Apr.2016. DOI: 10.1016/j.apenergy.2016.01.051.

[7] Z. Wanzhong, W. Gang, W. Chunyan, Y. Leiyan, L. Yufang, "Energy transfer and utilization efficiency of regenerative braking with hybrid energy storage system", *Journal of Power Sources*, vol. 427, pp. 174-183, July 2019. DOI: 10.1016/j.jpowsour.2019.04.083.

[8] A. Alamili, Y. Xue, F. Anayi, "An experimental and analytical study of the ultra-capacitor storage unit used in regenerative braking systems",

Energy Procedia, vol. 159, pp. 376-381, Feb. 2019. DOI: 0.1016/j.egypro.2018.12.073.

[9] L. Liang, W. Xiangyu, X. Rui, H. Kai, L. Xujian, "AMT downshifting strategy design of HEV during regenerative braking process for energy conservation", *Applied Energy*, vol. 183, pp. 914-925, Dec. 2016. DOI: doi.org/10.1016/j.apenergy.2016.09.031.

[10] L. Jiejunyi, W. D. Paul, R. Jiageng, Y. Haitao, W. Jinglai, Z. Nong, "Gearshift and brake distribution control for regenerative braking in electric vehicles with dual clutch transmission", *Mechanism and Machine Theory* 133(2019) 1-22, DOI: 10.1016/j.mechmachtheory.2018.08.013.

[11] https://www.sciencedirect.com/topics/engineering/peltier-effect.

[12] D. S. Hamed, J. Samad, K. Shahram, P. Samira, "A comprehensive exergy analysis of a prototype Peltier air-cooler; experimental investigation", *Renewable Energy*, Vol. 131, pp. 308-317, Feb. 2019. DOI: 10.1016/j.renene.2018.07.056.

[13] H. Wei, Z. Gan, Z. Xingxing, J. Jie, L. Guiqiang, Z. Xudong, "Recent development and application of thermoelectric generator and cooler", *Applied Energy* 143 (2015) 1-25, DOI: 10.1016/j.apenergy.2014.12.075.

[14] S. Manikandan, S. C. Kaushik, R. Yang, "Modified pulse operation of thermoelectric coolers for building cooling applications", *Energy Conversion and Management*, vol. 140, pp. 145-156, May 2017. DOI: 10.1016/j.enconman.2017.03.003.

[15] L. Ding, W. Ruochen, Y. Wei, Z. Weiqi, "Parametric study of a thermoelectric module used for both power generation and cooling", *Renewable Energy* 154 (2020) 542-552, DOI: 10.1016/j.renene.2020.03.045.

[16] S. Limei, Z. Wenshuai, L. Guanyu, T. Zhilong, L. Qingqing, C. Huanxin, H. Qingjun, "Performance enhancement investigation of thermoelectric cooler with segmented configuration", *Applied Thermal Engineering* 168 (2020) 114852, DOI: 10.1016/j.applthermaleng.2019.114852.

[17] T. Xiao-Xiao, A. Soheil, M. Hazim, K. Amr, P. Samira, J. Kittisak, "Proposing tube-bundle arrangement of tubular thermoelectric module as a novel air cooler", *Energy* 208 (2020) 118428, DOI: 10.1016/j.energy.2020.118428.

[18] Q. Changsheng, S. Wankai, "Comprehensive modeling for optimized design of a thermoelectric cooler with non-constant cross-section: Theoretical considerations", *Applied Thermal Engineering* 176 (2020) 115384, DOI: 10.1016/j.applthermaleng.2020.115384.

[19] K. H. Trevor, Z. Bin, L. Jie, X. Zhaojun, P. Gang, "Enhanced cooling by applying the radiative sky cooler to both ends of the thermoelectric cooler", *Energy Conversion and Management* 212 (2020) 112785, DOI: 10.1016/j.enconman.2020.112785.

[20] S. Dongfang, S. Limei, C. Huanxin, J. Bin, J. Desuan, L. Huanyu, Y. Yu, T. Jingchun, "Modeling and analysis of the influence of Thomson effect on microthermoelectric coolers considering interfacial and size effects", *Energy* 196(2020) 117116, DOI: 10.1016/j.energy.2020.117116.

[21] L. HoSung, "The Thomson effect and the ideal equation on thermoelectric coolers", *Energy* 56 (2013), 1-69, DOI: 10.1016/j.energy.2013.04.049.

[22] M. Mirmanto, S. Syahrul, Y. Wirdan, "Experimental performances of a thermoelectric cooler box with thermoelectric position variations", *Engineering Science and Technology, an International Journal* 22 (2019) 177-184, DOI: 10.1016/j.jestch.2018.09.006.

[23] D. S. Hamed, J. Samad, K. Shahram, "Novel experiments on COP improvement of thermoelectric air coolers", *Energy Conversion and Management* 187 (2019) 328-338, DOI: 10.1016/j.enconman.2019.03.025.

[24] K. Mahadevan, K. balaveera Reddy, "Design Data Handbook", 3rd edition, CBS Publishers, Delhi-32.